ACS OMEGA

http://pubs.acs.org/journal/acsodf

Article

Identification of Antitumor Active Constituents in *Polygonatum sibiricum* Flower by UPLC-Q-TOF-MS^E and Network Pharmacology

Zhuang-zhuang Huang,[▽] Xia Du,[▽] Cun-de Ma, Rui-rui Zhang, Wei-ling Gong, and Feng Liu*

Cite This: *ACS Omega* 2020, 5, 29755−29764

Read Online

ACCESS | Metrics & More | Article Recommendations

ABSTRACT: We aimed to investigate the material basis and mechanisms underlying the antitumor activity of *Polygonatum sibiricum* flower by ultra-performance liquid chromatography quadrupole time-of-flight mass spectrometry (UPLC-Q-TOF-MS^E). A compound−protein interaction network for cancer was constructed to identify potential drug targets, and then the Kyoto Encyclopedia of Genes and Genomes (KEGG) pathway analysis was conducted to elucidate the pathways involved in the antitumor activity of *P. sibiricum* flower. Subsequently, molecular docking was performed to determine whether the identified proteins are a target of the compounds of *P. sibiricum* flower. Sixty-four compounds were identified in *P. sibiricum* flower. Among these, 35 active constituents and 72 corresponding targets were found to be closely associated with the antitumor activity of *P. sibiricum* flower. By constructing and analyzing the compound−target−pathway network, five key compounds and 10 key targets were obtained. The five key compounds were wogonin, rhamnetin, dauriporphine, chrysosplenetin B, and 5-hydroxyl-7,8-panicolin. The 10 key targets were PIK3CG, AKT1, PTGS1, PTGS2, MAPK14, CCND1, TP53, GSK3B, NOS2, and SCN5A. In addition, 34 antitumor-related pathways were identified using the KEGG pathway analysis. To further verify the results of network pharmacology screening, molecular docking was performed with the five key compounds and the top three targets based on degree ranking, namely, PIK3CG, AKT1, and PTGS2; the results of molecular docking were consistent with those of network pharmacology. *P. sibiricum* flower can exert its antitumor activity via multicomponent, multitarget, and multichannel mechanisms of action. In this study, we identified the antitumor active constituents of *P. sibiricum* flower and their potential mechanisms of action.

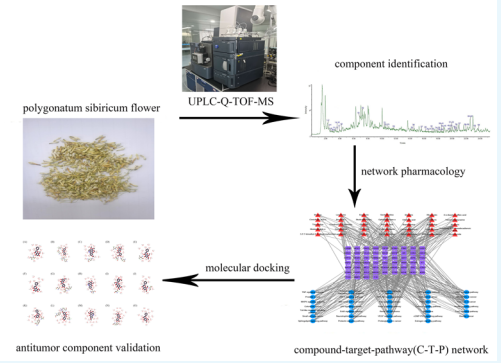

1. INTRODUCTION

Polygonatum sibiricum, also known as tendril leaf or Solomon's seal rhizome, is derived from the dried rhizome of *Polygonatum kingianum*, *Polygonatum* sp., or *Polygonatum cyrtonema* of the family Liliaceae.[1] It is distributed worldwide, including China, Japan, Korea, India, Russia, Europe, and North America; China is an abundant source of the species.[2] The use of *P. sibiricum* as both medicine and food was first recorded in Ming Yi Bie Lu (supplementary records of famous physicians).[3] Its rhizome replenishes the spleen, moistens the lungs, nourishes yin, and promotes body fluid secretion.[4] As it contains polysaccharides, saponins, flavones, lignans, amino acids, vitamins, alkaloids, and various trace elements, *P. sibiricum* is considered to have high medicinal and nutritional values.[5] As recorded in the Compendium of Materia Medica, the efficacy of various parts of *P. sibiricum* used in traditional medicine decreases in the following order: flower > fruit > rhizome.[6] Therefore, in this study, we aimed to comprehensively investigate the underutilized parts of *P. sibiricum* and its rhizome to increase their usage and reduce waste. We also aimed to identify the chemical composition of its flower.

As traditional Chinese medicines (TCMs) act through multicomponent synergistic effects,[7] it is necessary to study their individual chemical components, systematically and comprehensively. To achieve this goal, a reasonable and efficient analysis method meeting the requirements of rapid analysis while providing rich and accurate data must be selected. Ultra-performance liquid chromatography quadrupole time-of-flight mass spectrometry (UPLC-Q-TOF-MS^E) is a new analytical tool with good resolution, excellent sensitivity, and strong structural characterization capability.[8] Moreover, it can provide good separation and enable rapid and efficient analysis of some complex components. Furthermore, UPLC-Q-TOF-MS^E has been widely used in related fields, such as TCM component analysis and metabolomics.[9] In this study,

Received: July 27, 2020
Accepted: October 15, 2020
Published: November 15, 2020

https://dx.doi.org/10.1021/acsomega.0c03582
ACS Omega 2020, 5, 29755−29764

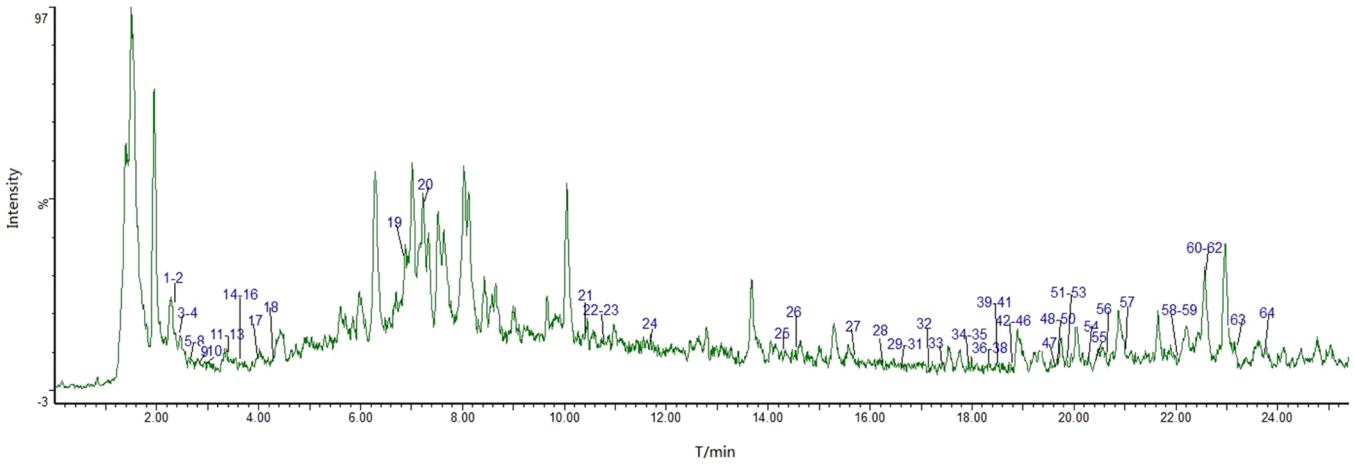

Figure 1. UPLC-Q-TOF-MS^E total ion current chromatogram of the 50% alcoholic extract of *Polygonatum sibiricum* flower in the positive ion mode.

we used UPLC-Q-TOF-MS^E combined with the UNIFI platform for the rapid qualitative analysis of the chemical composition of *P. sibiricum* flower. The results will provide a reference for quality control and material basis for the efficacy of *P. sibiricum*.

With rapid progress in the field of bioinformatics, network pharmacology has emerged as a powerful tool for the exploration of TCMs.[10] As network pharmacology provides a systematic understanding of medicine action and disease complexity, pharmacological models are beneficial for elucidating the effects of TCMs in particular diseases.[11] Therefore, in the present study, we combined network pharmacology to clarify the antitumor mechanism of *P. sibiricum* flower.

Recently, tumors have become an important topic of research as they are threatening human health worldwide. In the past few years, continuous upgrading of new tumor theories and the emergence of clinical medication problems such as tumor drug resistance have shifted the focus of cancer research toward the development of innovative anticancer drugs.[12] Screening of compounds with the potential to be developed as antitumor drugs has become a research hotspot during recent years.

Wang et al. developed stability-enhanced CM-camouflaged magnetic carbon nanotubes to screen drug leads in TCMs that target membrane receptors. A novel type of cell membrane-cloaked modified magnetic nanoparticles with good stability in drug discovery has been reported. High α1A-adrenergic receptor (α1A-AR) expressing HEK293 cell membrane-cloaked magnetic nanogrippers has been used as a platform for the specific targeting and binding of α1A-AR antagonists as candidate bioactive compounds in TCMs.[13,14] Therefore, exploring the antitumor mechanism of *P. sibiricum* flower will provide an important basis for research on new anticancer drugs.

2. RESULTS

2.1. Chemical Composition. The UNIFI data processing system was used to qualitatively analyze the 50% alcoholic extract of *P. sibiricum* flower; the total ion chromatogram (TIC) of ESI-MS in the positive ion mode is shown in Figure 1. We identified 64 compounds of five categories. These categories were flavonoids, alkaloids, terpenoids, saponins, and organic acids, with relatively more compounds from the first three categories. Table 1 contains the retention time, molecular formula, molecular ion peak, adduct ion, and cleavage fragment of the identified compounds. For sample processing, we investigated the 30, 50, and 70% methanolic extracts and found that the dissolution of the components of *P. sibiricum* flower was the highest in the 50% methanolic extract that was ultrasonically extracted for 30 min. The mobile phase systems, methanol−0.1% formic acid, acetonitrile−0.1% formic acid, and acetonitrile−0.1% acetic acid, were then compared to obtain the optimal mobile phase. As the separation of components was relatively better with acetonitrile−0.1% formic acid, we proceeded to compare the results of mass spectrometry with scanning in the positive and negative ion modes. The results showed a relatively good mass spectrometry response in the positive ion mode. UPLC-Q-TOF-MS^E has excellent sensitivity and good resolution, and the MS^E mass spectrometer mode allows simultaneous data collection with two scan functions via rapid switching between low-energy and high-energy collision scans.[15] Mass spectrometry was conducted using the Waters commercial database UNIFI, which performs automatic analyses of chemical components; moreover, it considerably simplifies the data processing operation.

2.2. Target Recognition and Disease Mapping. Target recognition of the 64 components was carried out using the PubChem, TCMSP, ETCM, and Batman-TCM databases. After duplicate removal, 294 targets were obtained for these compounds. Thereafter, "cancer/tumor" was entered as a keyword, and 894 targets were obtained from the TTD and Drugbank databases. A Venn analysis was performed using Venny 2.1 software to identify common compound targets and disease targets (see Figure 2). As a result, 72 targets were determined the potential targets of *P. sibiricum* flower extract, in terms of its antitumor activity.

2.3. KEGG Pathway Enrichment Analysis. Seventy-two targets were enriched in 81 pathways related to the antitumor effect, and 34 of the 81 pathways are closely related to tumors. Figure 3 shows the KEGG pathway analysis results of the antitumor effect of *P. sibiricum* flower. The results revealed that pathways in cancer, PI3K-Akt signaling pathway, and proteoglycans in cancer are the main pathways involved in the antitumor effect of *P. sibiricum* flower. The pathways in cancer had the highest number of antitumor-related targets; these included PIK3CG, AR, PTGS2, TP53, CDK2, MMP14, AKT1, CASP3, CCND1, HIF1A, CASP9, GSK3B, BCL2,

https://dx.doi.org/10.1021/acsomega.0c03582
ACS Omega 2020, 5, 29755−29764

Table 1. UPLC-Q-TOF-MS^E Results of the Chemical Constituents in the 50% Alcoholic Extract of *Polygonatum sibiricum* Flower

peak number	t_R/min	molecular formula	measured excimer ion peak (m/z)	mass number error (mDa)	adduct ion	fragment ion	compound
1	2.3	$C_{16}H_{12}O_5$	307.0584	0.71	+Na	270.0871, 251.028, 194.0291	wogonin
2	2.33	$C_{18}H_{17}NO_2$	302.1154	0.3	+Na	266.1569, 194.0291, 158.0892	roemerine
3	2.41	$C_7H_7NO_2$	138.0545	−0.42	+H		trigonelline
4	2.45	$C_7H_{13}NO_4$	198.0747	0.97	+Na	158.0771	norhyoscyamine
5	2.49	$C_9H_{17}NO_5$	242.1004	0.54	+Na	154.0835, 152.0671	vitamin B5
6	2.5	$C_5H_5N_5$	136.0614	−0.36	+H		adenine
7	2.51	$C_{20}H_{17}NO_5$	352.118	0.04	+H		dauriporphine
8	2.52	$C_{18}H_{13}NO_3$	292.0971	0.31	+H, +Na	234.0373, 185.0034, 176.069, 174.047	lysicamine
9	2.54	$C_7H_{13}NO_3$	182.079	0.28	+Na		2α, 3β, 4α-trihydroxyl desmethyl tropane
10	2.68	$C_{11}H_{21}NO_5$	248.1487	−0.59	+H	230.1377, 212.1267, 202.1427, 194.1154	pantothenic acid
11	3.36	$C_6H_6N_2O$	123.0545	−0.78	+H		nicotinamide
12	3.36	$C_{10}H_{13}N_5O_3$	274.0912	0.09	+Na	234.0938, 226.1111, 224.0882, 221.1266	cordycepin
13	3.37	$C_{18}H_{15}N_3O$	312.111	0.27	+Na, +H	273.1083, 264.1052, 259.0796, 245.0693	dihydrorutaecarpine
14	3.61	$C_{22}H_{28}O_9$	459.1634	0.82	+Na	324.153, 297.1014, 294.1521, 268.1032	bruceine I
15	3.65	$C_4H_6O_4$	119.033	−0.87	+H		succinic acid
16	3.66	$C_{10}H_{13}N_5O_4$	268.1035	−0.52	+H	235.1037, 209.0922, 179.079, 178.0667	adenosine
17	4.01	$C_5H_5N_5O$	152.0562	−0.54	+H		guanine
18	4.32	$C_{20}H_{23}NO_4$	342.1695	−0.53	+H	301.1331, 268.103, 257.1141, 175.0772	liriodendrin
19	6.91	$C_{20}H_{25}NO_3$	328.191	0.29	+H	282.1307, 264.1221, 250.1036, 204.0996	leonticine
20	7.24	$C_9H_{11}NO_2$	166.0858	−0.5	+H		gentiatibetine
21	10.45	$C_{23}H_{26}N_2O_4$	395.1964	−0.1	+H	355.1854, 341.1692	brucine
22	10.68	$C_{20}H_{23}N_7O_7$	474.1723	−0.88	+H	345.1294, 327.1161, 277.1204, 274.105	leucovorin
23	10.77	$C_{20}H_{30}O_4$	357.2033	−0.33	+Na	247.1013, 229.0955, 216.1223, 216.0864	preleoheterin
24	11.63	$C_8H_{12}N_2$	159.0904	1.13	+Na		ligustrazine
25	14.26	$C_{14}H_{12}O_{11}$	379.028	0.83	+Na		chebulic acid
26	14.54	$C_{21}H_{36}O_{10}$	449.238	−0.07	+H	407.2343, 377.1982, 371.2144, 362.2381	shionoside A
27	15.67	$C_9H_{12}O_4$	207.0632	0.47	+Na		eucommia glycol
28	16.27	$C_{33}H_{40}O_{20}$	757.2184	−0.14	+H	625.1764, 604.1644, 581.1474, 576.1561	quercetin-3-*o*-(2g-α-l-rhamnosyl)-rutinoside
29	16.5	$C_{17}H_{14}O_5$	321.0727	−0.64	+Na	283.0553, 281.0777, 267.0621, 267.0228	5-hydroxyl-7,8-panicolin
30	16.5	$C_{17}H_{14}O_6$	337.0687	0.45	+Na	283.0553, 267.0228, 255.0239, 221.0412	skullcapflavone I
31	16.59	$C_{39}H_{64}O_{14}$	757.4362	−0.64	+H	556.2605, 483.2986, 314.1236, 309.1183	timosaponin A-2
32	17.18	$C_{18}H_{14}O_6$	349.0683	0.09	+Na	310.0766, 298.0786, 295.0583, 203.0306	ophiopogonanone A
33	17.46	$C_{11}H_{15}NO_4$	248.0901	0.81	+Na	160.0739	lobeline B
34	17.97	$C_{15}H_{12}O_5$	295.0577	−0.04	+Na	255.0632, 243.0234, 242.0535, 165.0161	3-hydroxyl-2,8-dimethoxy xanthone
35	17.97	$C_{19}H_{16}O_7$	379.0789	0.09	+Na	341.0587, 325.0652, 313.0697, 311.0506	6-aldehydoisoophiopogonanone A
36	18.28	$C_{12}H_{17}NO_5$	278.1005	0.57	+Na	206.0801, 177.0527	lobeline A
37	18.33	$C_{18}H_{16}O_3$	303.0991	−0.09	+Na	191.0685, 189.0485, 187.034, 177.0527	6-methoxyl-2-(2-phenethyl)chromone
38	18.34	$C_{27}H_{30}O_{16}$	611.1605	−0.17	+H, +Na	722.2143, 633.1401, 625.1726, 616.1647	quercetin-3-*o*-neohesperidoside
39	18.49	$C_{18}H_{16}O_7$	367.0787	−0.08	+Na	313.0703, 311.0511, 299.0528, 297.0302	3,3′,7-trimethyl-4′,5-dihydroxyflavone
40	18.49	$C_{21}H_{20}O_{10}$	433.1128	−0.1	+H, +Na	415.102, 397.0916, 385.0875, 379.0811	cimicifugic acid E
41	18.5	$C_{23}H_{28}O_8$	433.1848	−0.92	+H	385.0875, 355.0761, 332.1304, 325.0686	pseudolaric acid
42	18.76	$C_{26}H_{30}O_{10}$	503.1915	0.32	+H	476.1716, 472.2123, 413.0907, 376.1593	(*R*)-shihulimonin A
43	18.77	$C_{11}H_{16}O_3$	219.0994	0.22	+Na		digiprolactone
44	18.83	$C_{16}H_{12}O_7$	317.0647	−0.91	+H	302.0409, 301.0244, 287.0539, 285.0372	eupatorin
45	18.98	$C_{19}H_{18}O_8$	397.0888	−0.54	+Na	343.0805, 341.0606, 328.0559, 327.0837	chrysosplenetin B
46	18.98	$C_{16}H_{13}O_6$	324.0596	−0.84	+Na	285.0374, 284.0619, 272.0638, 270.0484	peonidin
47	19.52	$C_{15}H_{10}O_6$	287.0543	−0.76	+H	269.0428, 163.0346	5,7,2′,5′-kaempferol
48	19.59	$C_{16}H_{12}O_7$	317.0649	−0.65	+H	302.0415, 301.0280, 299.0489, 285.0382	rhamnetin
49	19.59	$C_{11}H_{10}O_5$	245.0422	0.17	+Na	191.0296, 190.059, 190.0212, 189.0491	4-*o*-diacetyl-caffeic acid
50	19.6	$C_{18}H_{24}O_4$	327.1566	−0.1	+Na	217.0477, 203.0322, 153.0171, 151.0346	stylosin
51	19.67	$C_{19}H_{34}O_9$	407.2275	−0.08	+H	393.2091, 365.226, 317.1231, 295.1622	*Actinidia chinensis* ionone glycoside
52	19.7	$C_{20}H_{24}O_{11}$	463.1221	0.98	+Na	424.0958, 394.1716, 371.0672, 353.0569	ginkgolide c
53	19.73	$C_{27}H_{43}NO_2$	436.3193	0.69	+Na	358.2716, 341.2451, 340.2617, 339.2741	Hubei qin

https://dx.doi.org/10.1021/acsomega.0c03582
ACS Omega 2020, 5, 29755−29764

Table 1. continued

peak number	t_R/min	molecular formula	measured excimer ion peak (m/z)	mass number error (mDa)	adduct ion	fragment ion	compound
54	20.32	$C_{45}H_{72}O_{17}$	885.483	−1.26	+H	841.5004, 792.4200, 753.4486, 720.3719	pennogenin-3-*o*-*α*-l-rhamnopyranosyl-(1 → 2)-[*α*-l-rhamnopyranosyl(1 → 4)]-*β*-D-glucopyranoside
55	20.46	$C_{20}H_{28}O_5$	371.1836	0.75	+Na	295.1618, 249.0809, 213.1567, 201.122	14-desoxy-11-andrographolide
56	20.64	$C_{25}H_{22}O_9$	467.1336	−0.01	+H	453.1104, 451.0926, 423.1083, 409.0874	silandrin
57	21	$C_{11}H_{14}O_6$	243.0861	−0.26	+H	177.0541, 172.0821	lamiophlomiol B
58	22.15	$C_{16}H_{28}O_3$	291.193	−0.04	+Na	207.1354, 193.1534, 183.1479	13-hydroxyl-9,11-hexadecane dienoic acid
59	22.31	$C_{30}H_{40}N_4O_5$	537.3059	−1.27	+H	405.2535, 393.1469, 390.1975, 361.2546	ephedradine C
60	22.69	$C_{10}H_8O_3$	177.0543	−0.35	+H	163.072, 161.0567, 149.0566, 147.0395	erythrocentaurin
61	22.69	$C_9H_9NO_2$	186.0539	1.39	+Na	149.0566, 147.0395	gentianidine
62	22.75	$C_{36}H_{49}NO_{12}$	710.3147	0.03	+Na	639.2611, 614.2639, 580.2548, 567.2466	3-acetylaconitine
63	23.26	$C_{24}H_{30}O_{13}$	549.1574	−0.47	+Na	417.1140, 387.1071, 365.127, 329.0618	mudanpioside E
64	23.73	$C_{23}H_{26}O_{10}$	485.1427	0.86	+Na	321.0947, 303.0844, 255.0636, 235.0838	lactiflorin

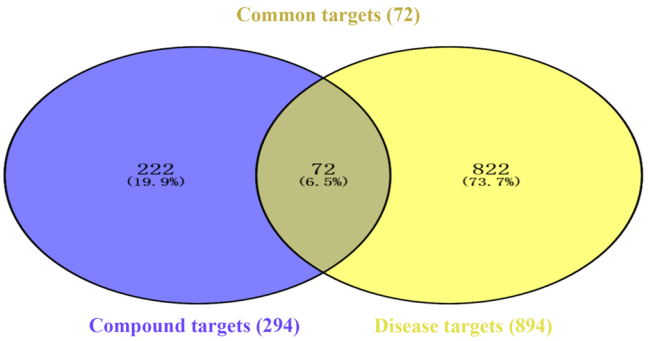

Figure 2. Venn diagram for the antitumor activity of *Polygonatum sibiricum* flower.

VEGFA, PRKACA, NOS2, and FN1. The PI3K-Akt signaling pathway had 14 antitumor-related targets, namely PIK3CG, MCL1, TP53, CDK2, KDR, AKT1, CCND1, CASP9, CHRM1, GSK3B, BCL2, VEGFA, INSR, and FN1. The proteoglycans in cancer had 13 targets related to the antitumor effect of *P. sibiricum* flower, namely PIK3CG, TNF, TP53, SRC, KDR, AKT1, CASP3, CCND1, HIF1A, MAPK14, VEGFA, PRKACA, and FN1.

2.4. Network Construction and Analysis. The C−T−P network of the *P. sibiricum* flower contained 127 nodes. In Figure 4, the 35 compounds are shown in red, 58 targets are shown in purple, and 34 pathways are shown in blue, and the 433 lines indicate the relationships among the compounds, targets, and pathways. Network analysis data were obtained

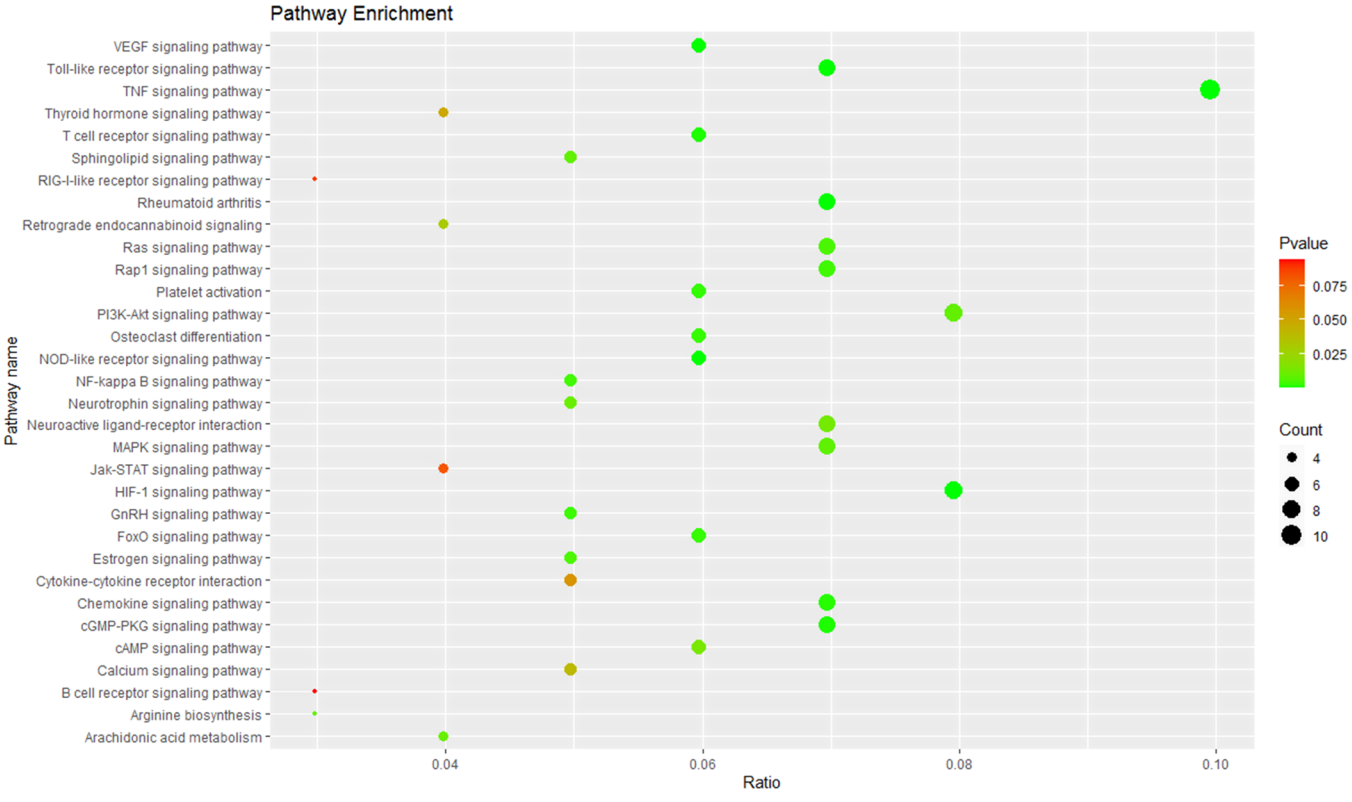

Figure 3. KEGG pathway enrichment analysis results for the antitumor activity of *Polygonatum sibiricum* flower.

https://dx.doi.org/10.1021/acsomega.0c03582
ACS Omega 2020, 5, 29755−29764

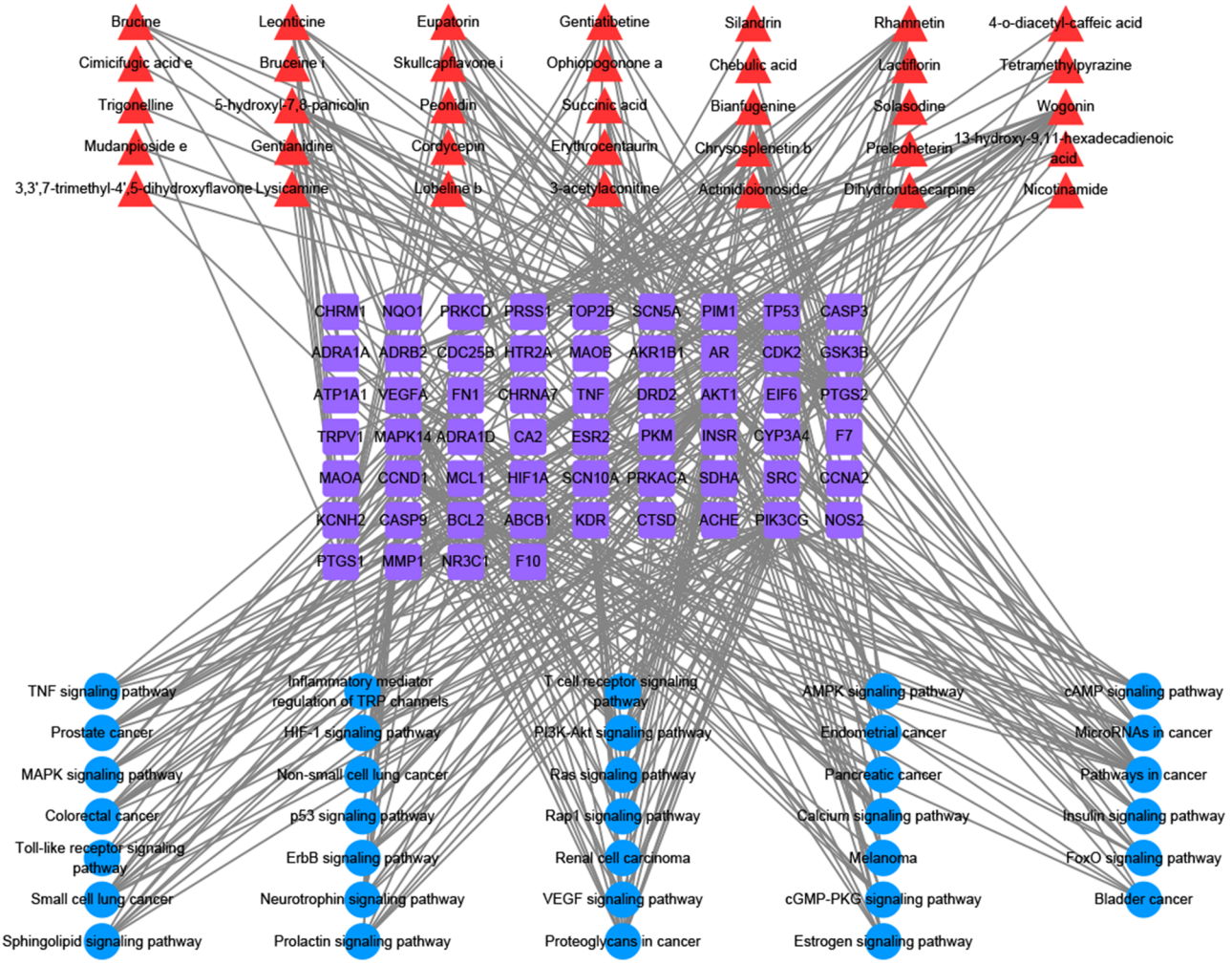

Figure 4. Compound−target−pathway (C−T−P) network for the antitumor activity of *Polygonatum sibiricum* flower.

using Cytoscape 3.8.0. Compounds and targets were screened based on degree and betweenness centrality, respectively. As shown in Table 2, five key compounds and 10 key targets with values above the mean were obtained. The three targets with the highest degree values among all targets were PI3-kinase gamma RAC-alpha (PIK3CG; degree = 33, betweenness centrality = 0.142, closeness centrality = 0.451), serine/threonine-protein kinase (AKT1; degree = 30, betweenness centrality = 0.092, closeness centrality = 0.412), and prostaglandin G/H synthetase 2 (PTGS2; degree = 28, betweenness centrality = 0.186, closeness centrality = 0.442), and they were associated with 33, 30, and 28 compounds, respectively. Based on the available literature, the above key compounds, wogonin, rhamnetin, and 5-hydroxyl-7,8-panicolin, and key targets, PIK3CG, AKT1, PTGS2, and PTGS1, were used to verify the antitumor components in *P. sibiricum* flower and their mechanisms of action.

2.5. Molecular Docking Results. Molecular docking was performed with five key compounds with the highest degree centrality for *P. sibiricum* flower and three core targets PIK3CG (PDB ID: 2A5U), AKT1 (PDB ID: 6HHH), and PTGS2 (PDB ID: 5IKR). The binding energy is shown in Table 4. To evaluate the binding ability of key compounds and key targets, we used the empirical threshold (−5.0 kcal/mol) mentioned in the literature as the evaluation standard.[16] If the docking binding energy was lower than the threshold, it showed that the binding ability between the target and compound was stronger. The results showed that the binding ability of all these key compounds to the three key targets was higher than the empirical threshold (Table 3). We further analyzed the interaction between the compounds and targets (see Figure 5).3). The results showed that the complexes of PIK3CG and all key components have hydrogen bonds, for example, three hydrogen bonds in the complex PIK3CG−wogonin, six hydrogen bonds in the complex PIK3CG−rhamnetin, one hydrogen bond in the complex PIK3CG−dauriporphine, five hydrogen bonds in the complex PIK3CG−chrysosplenetin B, and three hydrogen bonds in the complex PIK3CG−5-hydroxyl-7,8-panicolin. The binding energies of these complexes were lower than the threshold. AKT1 showed similar results. It is known that PIK3CG and AKT1 are closely related to the occurrence and development of tumors. These results were also consistent with the results of the KEGG pathway enrichment analysis.

3. DISCUSSION

Among these key compounds, wogonin is a natural flavonoid and is one of the main active constituents of *Scutellaria baicalensis*, used in TCMs.[17] Rong et al. reported that combining wogonin and sorafenib effectively kills human hepatocellular carcinoma cells via autophagy inhibition and potentiating apoptosis.[18] Moreover, wogonin, which is

https://dx.doi.org/10.1021/acsomega.0c03582
ACS Omega 2020, 5, 29755−29764

Table 2. Network Analysis Results of the Key Active Components, Key Targets, and Key Pathways for the Antitumor Activity of *Polygonatum sibiricum* Flower

no.	node name	degree centrality (DC)	betweenness centrality (BC)	closeness centrality (CC)
1	wogonin	24	0.136	0.458
2	rhamnetin	15	0.077	0.420
3	dauriporphine	15	0.050	0.393
4	chrysosplenetin B	13	0.048	0.393
5	5-hydroxyl-7,8-panicolin	12	0.023	0.406
6	PIK3CG	33	0.142	0.451
7	AKT1	30	0.092	0.412
8	PTGS2	28	0.186	0.442
9	PTGS1	17	0.044	0.393
10	MAPK14	17	0.047	0.398
11	CCND1	17	0.028	0.376
12	TP53	17	0.027	0.371
13	GSK3B	16	0.037	0.388
14	NOS2	13	0.036	0.390
15	SCN5A	12	0.037	0.378
16	pathways in cancer	17	0.058	0.429
17	PI3K-Akt signaling pathway	14	0.029	0.376
18	proteoglycans in cancer	13	0.026	0.381

Table 3. Docking Energy Results of the Complex between Key Targets and Key Compounds of *Polygonatum sibiricum* Flower

protein name	gene name	PDB ID	ligand name	binding energy (kcal/mol)
PI3-kinase gamma RAC-alpha	PIK3CG	2A5U	wogonin	−7.53
			rhamnetin	−7.92
			dauriporphine	−8.34
			chrysosplenetin B	−7.71
			5-hydroxyl-7,8-panicolin	−7.86
serine/threonine protein kinase	AKT1	6HHH	wogonin	−6.08
			rhamnetin	−6.19
			dauriporphine	−7.56
			chrysosplenetin B	−5.92
			5-hydroxyl-7,8-panicolin	−6.60
prostaglandin G/H synthetase 2	PTGS2	5IKR	wogonin	−6.22
			rhamnetin	−5.54
			dauriporphine	−7.28
			chrysosplenetin B	−5.82
			5-hydroxyl-7,8-panicolin	−6.77

extensively studied, has been reported to exert antitumor effects via several mechanisms, including intrinsic and extrinsic apoptotic signaling pathways, carcinogenesis diminution, telomerase activity inhibition, metastasis inhibition in the inflammatory microenvironment, anti-angiogenesis, cell growth inhibition, cell cycle arrest, and increased H_2O_2 generation and Ca^{2+} accumulation. It is also used as an adjuvant with anticancer drugs.[19] Wogonin induces the senescence of breast cancer cells by suppressing TXNRD2 expression; breast cancer remains the second most cause of cancer-related mortality in women. Among the breast cancers, triple-negative breast cancer (TNBC) has a more aggressive clinical course. It has been reported that in TNBC cell lines including MDA-MB-231 and 4T1 cells, wogonin (5,7-dihydroxy-8-methoxy-2-phenyl-4H-1-benzopyran-4-one) at moderate concentrations (50−100 μM) not only induced permanent proliferation inhibition but also increased P16 expression, β-galactosidase activity, senescence-associated heterochromatin foci, and SASP, which are typical characteristics of cellular senescence.[20] Rhamnetin is a flavonoid with antioxidant, anti-inflammatory, and antitumor effects. It has been reported that rhamnetin affects cell proliferation, and thus has the potential for being used in cancer treatment.[21] 5-Hydroxy-7,8-panicolin is a polymethoxy flavonoid and belongs to a class of flavonoids that has multiple methoxy groups, low polarity, a planar structure, and strong biological activities. Multimethoxyl flavonoids, a class of flavonoids, have been reported to possess strong antitumor activity. Chen and Dong evaluated the antitumor mechanisms of multimethoxyl flavonoids and found that they can inhibit the proliferation, infiltration, and metastasis of tumor cells and tumor angiogenesis.[22]

PTGS1 and PTGS2 are the targets of nonsteroidal anti-inflammatory drugs (NSAIDs), including aspirin and ibuprofen,[23−25] and the inhibition of PGHSs with NSAIDs acutely reduces inflammation, pain, and fever. Furthermore, long-term use of these drugs reduces fatal thrombotic events and the development of colon cancer and Alzheimer's disease. Chemotherapy with a single chemotherapeutic agent or a combined chemotherapeutic regimen is the clinically standardized treatment for almost all human cancers. Upregulated expression of cyclooxygenase (COX)-2, also known as prostaglandin-endoperoxide synthase (PTGS), is associated with human cancer development and progression; COX-2 inhibitors show antitumor activity in different human cancers.[26] Langsenlehner et al.[27] showed that the target, PTGS2, is closely related to a high risk of breast cancer, and Kosuke et al.[28] have shown that high expression of the PTGS2 receptor and the incidence of colon cancer have a certain degree of correlation. AKT1 is one of the three closely related serine/threonine protein kinases (AKT1, AKT2, and AKT3) called the AKT kinase, and it regulates many processes, including metabolism, proliferation, cell survival, growth, and angiogenesis.[29,30] The AKT pathway is a major regulator of human pancreatic adenocarcinoma progression and a key pharmacological target. In vivo pharmacological co-inhibition of AKT and mitochondrial metabolism effectively controlled pancreatic adenocarcinoma growth in preclinical models via de-differentiation and acquisition of stemness through c-Myc downregulation and NANOG upregulation, which are required for the survival of adapted cancer stem cell (CSCs).[31] *PIK3CG* is an upregulated gene and a subunit of PI3K, which is closely related to various tumors.[32] *AKT1* is a downregulated gene and is highly expressed in tumor tissues. It can participate in tumor metastasis.[33] Both these genes are involved in the PI3K/Akt cell transduction pathway, which can promote tumor development.[34]

The PI3K-Akt signaling pathway is an intracellular signaling pathway important for regulating the cell cycle and is activated

https://dx.doi.org/10.1021/acsomega.0c03582
ACS Omega 2020, 5, 29755−29764

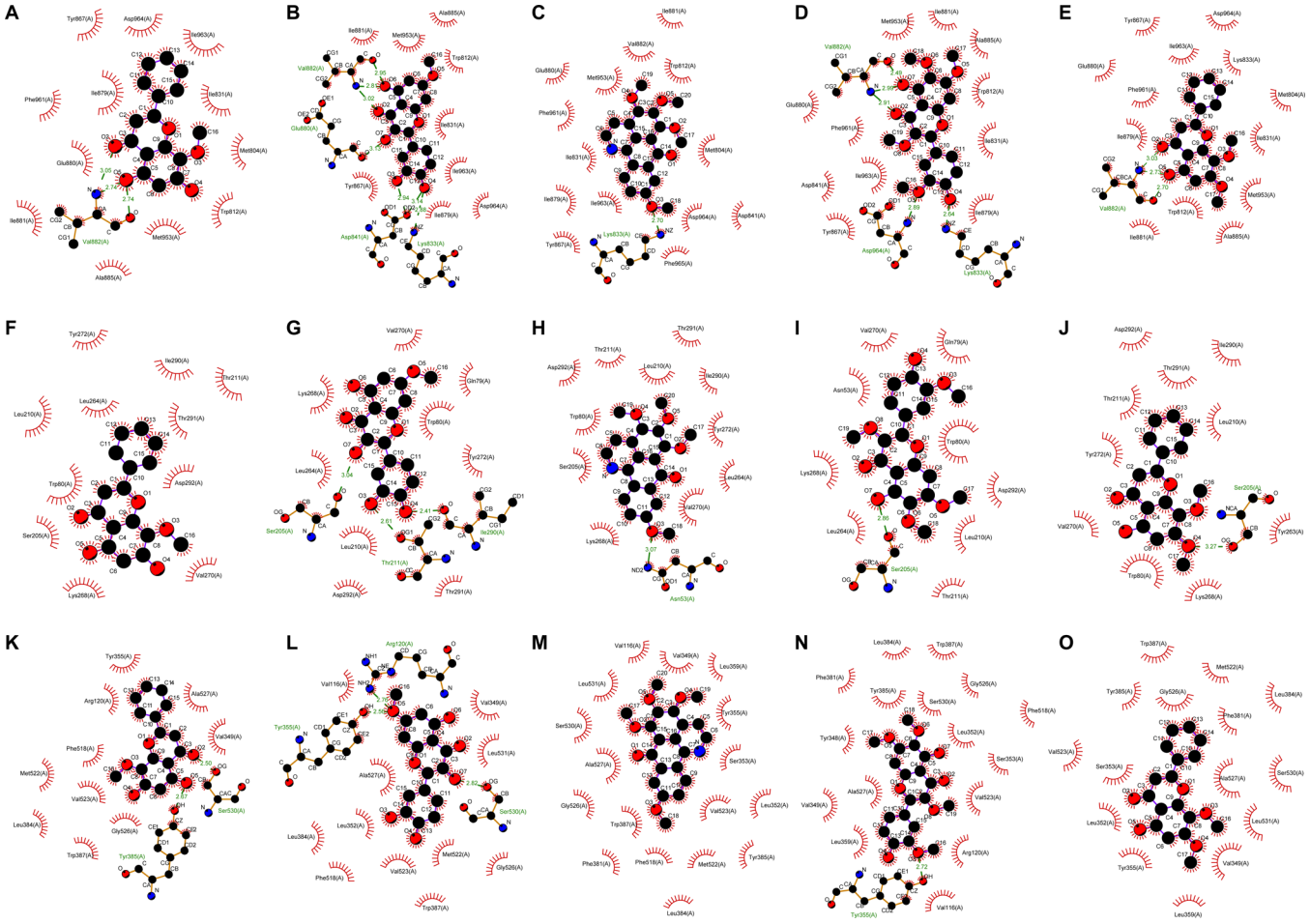

Figure 5. Interaction graphics between the compounds and targets: (A) PIK3CG−wogonin, (B) PIK3CG−rhamnetin, (C) PIK3CG−dauriporphine, (D) PIK3CG−chrysosplenetin B, (E) PIK3CG−5-hydroxyl-7,8-panicolin, (F) AKT1−wogonin, (G) AKT1−rhamnetin, (H) AKT1−dauriporphine, (I) AKT1−chrysosplenetin B, (J) AKT1−5-hydroxyl-7,8-panicolin, (K) PTGS2−wogonin, (L) PTGS2−rhamnetin, (M) PTGS2−dauriporphine, (N) PTGS2−chrysosplenetin B, and (O) PTGS2−5-hydroxyl-7,8-panicolin.

by different types of cellular stimuli or toxic insults. The PI3K-Akt signaling pathway plays an important role in the antitumor effect of *P. sibiricum* flower (degree = 14, betweenness centrality = 0.029, closeness centrality = 0.376). AKT overexpression or activation may lead to an increased response to ambient levels of growth factors. Sustained activation of AKT makes tumor cells insensitive to antiproliferative signals by inducing the nuclear entry of Mdm2, which leads to the inhibition of p53-regulated processes, and by inducing cytoplasmic localization of p21Cip/Waf1 and p27Kip, which promotes cell proliferation. AKT activation also suppresses the apoptosis of cancer cells by inactivating pro-apoptotic factors Bad and pro-caspase-9, but activating IKK induces the transcription of NFκB-regulated antiapoptotic genes. In addition, the PI3K-Akt pathway also promotes tumor angiogenesis via eNOS activation and contributes to invasiveness by inhibiting anoikis and stimulating MMP secretion.[35−37] These results indicate the involvement of multicomponent, multitarget, and multichannel characteristics in the antitumor activity of *P. sibiricum* flower.

4. CONCLUSIONS

We integrated UPLC-Q-TOF-MS^E with the UNIFI natural product information platform to perform a rapid qualitative analysis of the chemical constituents of *P. sibiricum* flower. From this, we identified 64 compounds; then, we employed network pharmacology methods for target recognition, pathway analysis, and network construction. This methodology was employed to explain, to the best of our knowledge, for the first time, the material basis for the efficacy and molecular mechanisms of the antitumor effect of *P. sibiricum* flower. Five key active components and 10 key targets were obtained, and 34 main pathways were identified via the KEGG pathway analysis. The findings reflect the multicomponent, multitarget, and multichannel characteristics of TCMs.

5. MATERIALS AND METHODS

5.1. Chemical Composition Analysis of *Polygonatum sibiricum* Flower. *5.1.1. Instrument and Materials.* A Waters Acquity ultra-high-performance liquid chromatography System (UHPLC; Waters, U.S.A.), quadrupole time-of-flight mass spectrometer (Q-TOF-MS) (Waters, U.S.A), AR1140 electronic analytical balance (Mettler, Switzerland), acetonitrile (Fisher), methanol (Fisher), formic acid (Sigma, U.S.A), leucine encephalin (Waters), sodium formate (Sigma), a Millipore ultrapure water machine (Millipore, U.S.A.), and *P. sibiricum* flower (*Polygonatum sibiricum* GAP base) were used in the study.

5.1.2. Preparation of Sample Solution. Approximately 2.0 g of *P. sibiricum* flower (dried and powdered) was added to 50

https://dx.doi.org/10.1021/acsomega.0c03582
ACS Omega 2020, 5, 29755−29764

mL of 50% methanol for ultrasonic extraction for 30 min. The solution was filtered, and the filtrate obtained was passed through a 0.22 μm filter membrane to obtain the sample solution.

5.1.3. UPLC Conditions. We used the Waters ACQUITY UPLC BEH C18 (4.6 mm × 100 mm, 1.7 μm) column for the analysis and performed gradient elution with 0.5% formic acid in water (A)−acetonitrile (B) as the mobile phase. We employed the following gradient: 0−4 min, 5−10% B; 4−12 min, 10−20% B; 12−16 min, 20−30% B; 16−18 min, 30−30% B; 18−20 min, 30−5% B; and 20−25 min, 5−5% B. The column temperature was 40 °C, flow rate was 0.10 mL/min, and injection volume was 10 μL.

5.1.4. MS Test Conditions. Electrospray ionization (ESI) was used in the positive ion mode with the following conditions: volume flow rate of nebulizer gas (N_2), 800 L/h; temperature of the solvent-removing gas, 450 °C; gas flow rate of the cone, 50 L/h; temperature of the ion source, 120 °C; capillary voltage, 3.0 kV; cone voltage, 40 V; and ion spray voltage (ESI+), 3000 V. The MS^E test was performed in the scan mode with a scan range of m/z 100−1500; leucine enkephalin was used as the accurate mass number for the calibration solution.

5.1.5. Data Collection and Processing. Data were collected in the MS^E mass spectrometry mode. The collected raw format data file was imported into UNIFI software, with the Waters commercial database; then, the collected data were automatically matched and passed through a preset workflow and molecular sieve. The compound name, molecular formula, structural formula, retention time, and fragment ion theoretical exact mass number required in the UNIFI entry were selected, and the main compounds were manually identified and confirmed by combining offline and online mass spectrometry databases (PubMed, MassBank, Chemspider, and METLIN) and relevant literature.[38]

5.2. Mechanism Study by Network Pharmacology. *5.2.1. Target Fishing and Disease Mapping.* The structure of all identified components was obtained from the PubChem database (https://pubchem.ncbi.nlm.nih.gov/). The structure of potential targets was obtained from the TCMSP (https://tcmspw.com/tcmsp.php), Batman-TCM (http://bionet.ncpsb.org/batman-tcm/), and ETCM (http://www.tcmip.cn) databases. All TCMSP drug targets were imported into the UniProt (https://www.uniprot.org/) database; the target gene name was entered to define the species as "*Homo sapiens*", and all protein names were corrected to their official names (official symbol). To obtain the antitumor active constituents and the corresponding targets of *P. sibiricum* flower, the targets were mapped to the tumor and its related diseases by searching the TTD (http://db.idrblab.net/ttd/) and Drugbank (https://www.drugbank.ca/) bioinformatic databases. All targets were converted using the UniProt database and corrected to the standard abbreviations.

5.2.2. Kyoto Encyclopedia of Genes and Genomes (KEGG) Analysis. To determine the molecular mechanism underlying the antitumor effect of *P. sibiricum* flower, The KEGG pathway analysis was performed using DAVID (https://david.ncifcrf.gov/). We used an automated method for the functional annotation of gene lists. All targets related to the antitumor effects were added to the submitted gene list, and then the target genes were selected to identify the source. A Gene ID conversion tool was used to ensure all targets met the requirements. Subsequently, the list to DAVID, as a new converted list, was resubmitted. The target enrichment results of the KEGG pathways were obtained using functional annotation tools.

5.2.3. Network Construction and Analysis. The compound−target−pathway (C−T−P) network was constructed using Cytoscape 3.8.0, which is an open-source software for visualizing complex networks and integrating these with any type of attribute data. In the network, the compounds, targets, and pathways are represented by nodes, and the interaction between two nodes is represented by an edge. In addition, the importance of each node in the networks was evaluated using a crucial topological parameter, namely degree. The topological properties were analyzed using the Network Analyzer plug-in for Cytoscape to confirm the key components and targets, such as degree centrality (DC), betweenness centrality (BC), and closeness centrality (CC).

5.3. Molecular Docking. Molecular docking was performed to verify the interactions between some compounds and targets. The structure of the compounds was obtained from the PubChem database (https://pubchem.ncbi.nlm.nih.gov). The structure of the targets was obtained from the PDB database (http://www.pdb.org). Docking simulation was performed using AutoDock 4.2 software. During the docking calculations, gasteiger charges and hydrogen atoms were added to the proteins using the automated docking tool. The auxiliary program Autogrid was used to set the docking boxes, which were defined according to the crystal structures of protein complexes with known ligands. Lamarckian genetic algorithm (LGA) was adopted for each docking progress.

AUTHOR INFORMATION

Corresponding Author

Feng Liu − *Shaanxi Institute of International Trade & Commence, Xi'an 712046, China; Collaborative Innovation Center of Green Manufacturing Technology for Traditional Chinese Medicine in Shaanxi province, Xi'an 710075, China;* orcid.org/0000-0001-7811-038X; Email: liufeng1720@163.com

Authors

Zhuang-zhuang Huang − *Shaanxi Institute of International Trade & Commence, Xi'an 712046, China; Shaanxi Buchang Pharmaceutical Co. Ltd., Xi'an 710075, China;* orcid.org/0000-0001-7262-2819

Xia Du − *Shaanxi Academy of Traditional Chinese Medicine, Xi'an, Shaanxi 710003, China; Center for Post-Doctoral Studies, China Academy of Chinese Medical Sciences, Beijing 100700, China;* orcid.org/0000-0002-6474-6579

Cun-de Ma − *Shaanxi Buchang Pharmaceutical Co. Ltd., Xi'an 710075, China;* orcid.org/0000-0002-0873-6042

Rui-rui Zhang − *Shaanxi Institute of International Trade & Commence, Xi'an 712046, China;* orcid.org/0000-0002-0931-8854

Wei-ling Gong − *Shaanxi University of Chinese Medicine, Xi'an 712046, China;* orcid.org/0000-0002-5658-3968

Complete contact information is available at: https://pubs.acs.org/10.1021/acsomega.0c03582

Author Contributions

[▽]Z.Z.H. and X.D. contributed equally to this study.

Notes

The authors declare no competing financial interest.

https://dx.doi.org/10.1021/acsomega.0c03582
ACS Omega 2020, 5, 29755−29764

■ ACKNOWLEDGMENTS

The work was supported by the Key R&D Program Projects in Shaanxi Province (grant number 2018SF-327) and the Youth Innovation Team of Shaanxi Universities Shajiao (2019) No. 90. The funder had no role in designing the study; collecting, analyzing, and interpreting the data; writing the manuscript; and submitting the manuscript for publication.

■ REFERENCES

(1) Cui, X.; Wang, S.; Cao, H.; Guo, H.; Li, Y.; Xu, F.; Zheng, M.; Xi, X.; Han, C. A Review: The Bioactivities and Pharmacological Applications of Polygonatum sibiricum polysaccharides. *Molecules* **2018**, *23*, 1170.

(2) Li, L.; Tian, L. N.; Ren, Z. X.; Long, Z. J. Research progress on the structural analysis and functional activity of polysaccharides. *Chin. J. Exp. Tradit. Med. Fromul* **2015**, *21*, 231−234.

(3) Chen, H.; Feng, S. S.; Sun, Y. J.; Hao, Z. Y.; Feng, W. S.; Zheng, X. K. Research progress in the chemical constituents and pharmacological activities of three Polygonatum species. *Chin. Tradit. Herbal Drugs* **2015**, *46*, 2329−2338.

(4) Jiang, W.; Ye, C. S.; Wu, Z. G.; Tao, Z. M. Herbal research on *Polygonatum sibiricum*. *Chin. Med. Mat.* **2017**, *40*, 2713−2716.

(5) Zhao, H.; Wang, Q. L.; Hou, S. B.; Chen, G. Chemical constituents from the rhizomes of *Polygonatum sibiricum* Red. and anti-inflammatory activity in RAW264.7 macrophage cells. *Nat. Prod. Res.* **2019**, *33*, 2359−2362.

(6) Zhao, W. L.; Zhao, Y.; Yiider, T. S. Research progress in effects of *Polygonatum sibiricum*. *Chin. Tradit. Herbal Drugs* **2018**, *49*, 4439−4445.

(7) Yang, Y.; Zhang, Z.; Li, S.; Ye, X.; Li, X.; He, K. Synergy effects of herb extracts: Pharmacokinetics and pharmacodynamic basis. *Fitoterapia* **2014**, *92*, 133−147.

(8) Kang, L. P.; Yu, K.; Zhao, Y.; Liu, Y. X.; Yu, H. S.; Pang, X.; Xiong, C. Q.; Tan, D. W.; Gao, Y.; Liu, C.; Ma, B. P. Characterization of steroidal glycosides from the extract of Paris Polyphylla var Yunnanensis by UPLC/Q-TOF MS^E. *J. Pharm. Biomed. Anal.* **2012**, *62*, 235−249.

(9) Lin, S.; Yue, X.; Ouyang, D.; Li, Q.; Yang, P. The profiling and identification of chemical components, prototypes and metabolites of Run-zao-zhi-yang capsule in rat plasma, urine and bile by an UPLC-Q-TOF/MS^E-based high-throughput strategy. *Biomed. Chromatogr.* **2018**, *12*, e4261.

(10) Yu, G.; Wang, W.; Wang, X.; Xu, M.; Zhang, L.; Ding, L.; Guo, R.; Shi, Y. Network pharmacology-based strategy to investigate pharmacological mechanisms of Zuojinwan for treatment of gastritis. *BMC Complementary Altern. Med.* **2018**, *18*, 292.

(11) Cao, H.; Li, S.; Xie, R.; Xu, N.; Qian, Y.; Chen, H.; Hu, Q.; Quan, Y.; Yu, Z.; Liu, J.; Xiang, M. Exploring the mechanism of Dangguiliuhuang decoction against hepatic fibrosis by network pharmacology and experimental validation. *Front. Pharmacol.* **2018**, *9*, 187.

(12) Olgen, S. Overview on anticancer drug design and development. *Curr. Med. Chem.* **2018**, *25*, 1704−1719.

(13) Hu, Q.; Bu, Y.; Cao, R.; Zhang, G.; Xie, X.; Wang, S. Stability designs of cell membrane cloaked magnetic carbon nanotubes for improved life span in screening drug leads. *Anal. Chem.* **2019**, *91*, 13062−13070.

(14) Bu, Y.; Hu, Q.; Zhang, X.; Li, T.; Xie, X.; Wang, S. A novel cell membrane-cloaked magnetic nanogripper with enhanced stability for drug discovery. *Biomater. Sci.* **2020**, *8*, 673−681.

(15) Pang, X.; Kang, L.; Yu, H.; Zhao, Y.; Xiong, C.; Zhang, J.; Shan, J.; Ma, B. Rapid isolation of new furostanol saponins from fenugreek seeds based on ultra-performance liquid chromatography coupled with a hybrid quadrupole time-of-flight tandem mass spectrometry. *J. Sep. Sci.* **2012**, *35*, 1538−1550.

(16) Zhou, W.; Wang, J.; Wu, Z.; Huang, C.; Lu, A.; Wang, Y. Systems pharmacology exploration of botanic drug pairs reveals the mechanism for treating different diseases. *Sci. Rep.* **2016**, *6*, 36985.

(17) Zhao, Y.; Zhang, L.; Wu, Y.; Dai, Q.; Zhou, Y.; Li, Z.; Yang, L.; Guo, Q.; Lu, N. Selective anti-tumor activity of wogonin targeting the Warburg effect through stablizing p53. *Pharmacol. Res.* **2018**, *135*, 49−59.

(18) Rong, L. W.; Wang, R. X.; Zheng, X. L.; Feng, X. Q.; Zhang, L.; Zhang, L.; Lin, Y.; Li, Z. P.; Wang, X. Combination of wogonin and sorafenib effectively kills human hepatocellular carcinoma cells through apoptosis potentiation and autophagy inhibition. *Oncol. Lett.* **2017**, *13*, 5028−5034.

(19) Kumar, R.; Harilal, S.; Parambi, D. G. T.; Narayanan, S. E.; Uddin, M.; Marathakam, A.; Jose, J.; Mathew, G. E.; Mathew, B. Fascinating chemo preventive story of wogonin: A chance to hit on the head in cancer treatment. *Curr. Pharm. Des.* **2020**, DOI: 10.2174/1385272824999200427083040.

(20) Yang, D.; Guo, Q.; Liang, Y.; Zhao, Y.; Tian, X.; Ye, Y.; Tian, J.; Wu, T.; Lu, N. Wogonin induces cellular senescence in breast cancer via suppressing TXNRD2 expression. *Arch. Toxicol.* **2020**, *94*, 3433.

(21) Lan, L.; Wang, Y.; Pan, Z.; Wang, B.; Yue, Z.; Jiang, Z.; Li, L.; Wang, C.; Tang, H. Rhamnetin induces apoptosis in human breast cancer cells via the miR-34a/Notch-1 signaling pathway. *Oncol. Lett.* **2019**, *17*, 676−682.

(22) Chen, S.; Dong, Y. Advances in anti-tumor effect of multimethoxyl flavonoids. *Chin. Pharmacol. Bull.* **2017**, *33*, 1493−1495.

(23) Orlando, B. J.; Malkowski, M. G. Crystal structure of rofecoxib bound to human cyclooxygenase-2. *Acta Crystallogr. F Struct. Biol. Commun.* **2016**, *72*, 772−776.

(24) Lucido, M. J.; Orlando, B. J.; Vecchio, A. J.; Malkowski, M. G. crystal structure of aspirin-acetylated human cyclooxygenase-2: Insight into the formation of products with reversed stereochemistry. *Biochemistry* **2016**, *55*, 1226−1238.

(25) Orlando, B. J.; Malkowski, M. G. Substrate-selective inhibition of cyclooxygeanse-2 by fenamic acid derivatives is dependent on peroxide tone. *J. Biol. Chem.* **2016**, *291*, 15069−15081.

(26) Li, S.; Jiang, M.; Wang, L.; Yu, S. Combined chemotherapy with cyclooxygenase-2 (COX-2) inhibitors in treating human cancers: Recent advancement. *Biomed. Pharmacother.* **2020**, *129*, 110389.

(27) Langsenlehner, U.; Yazdani-Biuki, B.; Eder, T.; Renner, W.; Wascher, T. C.; Paulweber, B.; Weitzer, W.; Samonigg, H.; Krippl, P. The cyclooxygenase-2 (PTGS2) 8473T>C polymorphism is associated with breast cancer risk. *Clin. Cancer Res.* **2006**, *12*, 1392−1394.

(28) Mima, K.; Nishihara, R.; Yang, J.; Dou, R.; Masugi, Y.; Shi, Y.; da Silva, A.; Cao, Y.; Song, M.; Nowak, J.; Gu, M.; Li, W.; Morikawa, T.; Zhang, X.; Wu, K.; Baba, H.; Giovannucci, E. L.; Meyerhardt, J. A.; Chan, A. T.; Fuchs, C. S.; Qian, Z. R.; Ogino, S. MicroRNA MIR21 (miR-21) and PTGS2 expression in colorectal cancer and patient survival. *Clin. Cancer Res.* **2016**, *22*, 3841−3848.

(29) Hers, I.; Vincent, E. E.; Tavaré, J. M. Akt signalling in health and disease. *Cell Signal.* **2011**, *23*, 1515−1527.

(30) Heron-Milhavet, L.; Khouya, N.; Fernandez, A.; Lamb, N. J. Akt1 and Akt2: differentiating the aktion. *Histol. Histopathol.* **2011**, *26*, 651−662.

(31) Arasanz, H.; Hernández, C.; Bocanegra, A.; Chocarro, L.; Zuazo, M.; Gato, M.; Ausin, K.; Santamaría, E.; Fernández-Irigoyen, J.; Fernandez, G.; Santamaria, E.; Rodríguez, C.; Blanco-Luquin, I.; Vera, R.; Escors, D.; Kochan, G. Profound reprogramming towards stemness in pancreatic cancer cells as adaptation to AKT inhibition. *Cancers* **2020**, *12*, 2181.

(32) Chang, J.; Hong, L.; Liu, Y.; Pan, Y.; Yang, H.; Ye, W.; Xu, K.; Li, Z.; Zhang, S. Targeting PIK3CG in combination with paclitaxel as a potential therapeutic regimen in claudin-low breast cancer. *Cancer Manag. Res.* **2020**, *Volume 12*, 2641−2651.

(33) López-Cortés, A.; Leone, P. E.; Freire-Paspuel, B.; Arcos-Villacís, N.; Guevara-Ramírez, P.; Rosales, F.; Paz-Y-Miño, C. Mutational analysis of oncogenic AKT1 gene associated with breast cancer risk in the high-altitude Ecuadorian Mestizo population. *Biomed. Res. Int.* **2018**, *2018*, 1−10.

https://dx.doi.org/10.1021/acsomega.0c03582
ACS Omega 2020, 5, 29755−29764

(34) Vara, J. A. F.; Casado, E.; de Castro, J.; Cejas, P.; Belda-Iniesta, C.; González-Barón, M. PI3K/Akt signalling pathway and cancer. *Cancer Treat. Rev.* **2004**, *30*, 193−204.
(35) Chen, Y.-T.; Huang, C.-R.; Chang, C.-L.; Chiang, J. Y.; Luo, C.-W.; Chen, H.-H.; Yip, Y.-K. Jagged2 progressively increased expression from stage I to III of bladder cancer and melatonin-mediated downregulation of Notch/Jagged2 suppresses the bladder tumorigenesis via inhibiting PI3K/AKT/mTOR/MMPs signaling. *Int. J. Biol. Sci.* **2020**, *16*, 2648−2662.
(36) Yu, X.; Fan, H.; Jiang, X.; Zheng, W.; Yang, Y.; Jin, M.; Ma, X.; Jiang, W. Apatinib induces apoptosis and autophagy via the PI3K/AKT/mTOR and MAPK/ERK signaling pathways in neuroblastoma. *Oncol. Lett.* **2020**, *20*, 52.
(37) du Rusquec, P.; Blonz, C.; Frenel, J. S.; Campone, M. Targeting the PI3K/Akt/mTOR pathway in estrogen-receptor positive HER2 negative advanced breast cancer. *Ther. Adv. Med. Oncol.* **2020**, 175883592094093.
(38) Dudkin, A. V.; Morozik, Y. I.; Rybal'chenko, I. V.; Terentyev, A. G. Determination of the structure of alkyl radicals in a series of highly toxic organophosphorus compounds using mass spectrometry databases and library search. *J. Anal. Chem.* **2018**, *73*, 1275−1281.

https://dx.doi.org/10.1021/acsomega.0c03582
ACS Omega 2020, 5, 29755−29764